Online ISSN:- 1387-7003
Print ISSN:- 1387-7003

Inorganic Chemistry Communications 99 (2019) 20–25

Contents lists available at ScienceDirect

Inorganic Chemistry Communications

journal homepage: www.elsevier.com/locate/inoche

Short communication

Ni^{2+} substituted Mg-Cu-Zn ferrites by molten salt route: Evaluation of structural, morphological and electromagnetic properties

L.M. Thorat[a], J.Y. Patil[a], D.Y. Nadargi[a], R.C. Kambale[b], S.S. Suryavanshi[a,*]

[a] School of Physical Sciences, Solapur University, Solapur 413255, Maharashtra, India
[b] Department of Physics, Savitribai Phule Pune University, Pune 411007, Maharashtra, India

GRAPHICAL ABSTRACT

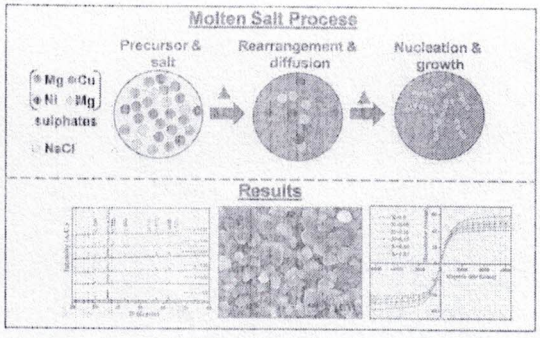

ARTICLE INFO

Keywords:
Ferrites
Molten salt
Magnetic materials
X-ray diffraction
TEM

ABSTRACT

We report a facile molten salt route to synthesize Ni^{2+} substituted Mg-Cu-Zn spinel ferrites with their electromagnetic properties. The ferrite nanoparticles ($Mg_{0.25-x}Ni_xCu_{0.25}Zn_{0.5}Fe_2O_4$ with x = 0.0–0.25 in step 0.05) synthesized at 800 °C using sodium chloride as a growth inhibitor, revealed an excellent tuning in electromagnetic properties due to addition of Ni. Single-phase formation of spinel ferrite having crystallite size in the range of 45–49 nm was observed by XRD and confirmed by TEM/SAED spot pattern. The obtained dielectric and magnetic properties (high initial permeability = 592, saturation magnetization = 325 emu, coercivity = 36.86 G) of nanostructured spinel ferrite suggest the possibility of utilization of the developed material for MLCI application. The molten salt chemistry, and thereby its effect on structural, morphological and electromagnetic properties of Mg-Cu-Zn ferrites are discussed.

1. Introduction

Currently, spinel ferrites have attracted wide attention due to their diverse applications in varieties of electromagnetic devices [1–7]. Specially, Mg-Cu-Zn ferrites are the potential material for multilayer chip inductor (MLCI) components and surface mount devices (SMD) due to their moderate soft magnetic nature with high electrical resistivity at high frequencies. In state-of-the-art, Shan and co-workers reported the magnetic properties of $NiFe_2O_4$with different morphologies. $NiFe_2O_4$ nano-spheres, rods, and octahedrons were developed using a facile hydrothermal method without any surfactant [8]. Monodisperse $NiFe_2O_4$ nanoparticles and their magnetic properties were developed investigated by Lasheras et al. using thermal decomposition route [9]. Likewise, Xu et al. reported the preparation of Co(II),

* Corresponding author.
E-mail address: sssuryavanshi@rediffmail.com (S.S. Suryavanshi).

https://doi.org/10.1016/j.inoche.2018.11.003
Received 4 October 2018; Received in revised form 25 October 2018; Accepted 1 November 2018
Available online 02 November 2018

Ni(II), Zn(II) spinel ferrites by surfactant-free solvothermal process for gas-sensing applications [10]. These synthetic strategies are certainly very appropriate for low volume production/applications of ferrites. To overcome the narrow production volume, numerous complementary techniques are available, viz. glycine/citrate combustion, pyrolysis, and molten salt technique (MSS) [11–17]. M. Salavati-Niasari et al. reported the various metal oxides and ferrites using aforementioned synthesis strategies. The work encompasses manganese(II), cobalt(II), nickel(II), copper(II), and zinc(II) complexes, and their ferrites [12–16]. Among the different synthesis techniques, the MSS (uses simple metal salts) is a traditional and well developed synthetic process.

Therefore here, the traditional route is readily extended to develop the ($Mg_{0.25-x}Ni_xCu_{0.25}Zn_{0.5}Fe_2O_4$ ($0 \le x \le 0.25$)) ferrites by MSS, and investigated the structural and electromagnetic properties. Further, the motivation behind incorporation of Ni^{2+} in place of Mg^{2+} is its higher magnetic moment ($2.83\mu_B$) compared to Mg^{2+} ($2.00\mu_B$), which will certainly improve the properties of targeted application, where low eddy currents losses, high electrical resistivity, high μ_i, and Ms, are important requisites.

2. Experimental details

In a typical synthesis, divalent metal precursors in sulphates form for Mg/Ni/Cu/Zn, $Fe(NO_3)_3{\cdot}9H_2O$, NaOH and NaCl were dry mixed in the molar ratio of 1:2:8:10, and grounded together in an agate mortar for ~30 min. During the mixing, the reaction started voluntarily, accompanied by the release of heat. As an exothermic reaction advanced, the synthetic mixture became mushy and underwent to gradual change of colorless-to-black. The mixture was then heated at 800 °C for 2 h (melting point of NaCl as a growth inhibitor) and subsequently cooled down to room temperature. Finally, the samples were thoroughly washed with distilled water, and dried under IR lamp. This powder was then made into pellets and toroids, followed by sintering at 950 °C (4 h) in air, to get the proper phase formation of Mg/Ni/Cu/Zn ferrite.

3. Results and discussion

Fig. 1 depicts the X-ray diffraction (XRD) patterns of synthesized Ni^{2+} substituted Mg-Cu-Zn ferrites. XRD signatures confirm the cubic spinel structure in accordance with JCPDS card: 08-0234. The broad and well resolved peaks in XRD reveal the crystalline nature having well-defined fine grains. The lattice constant (Table 1) was found to be increasing with Ni^{2+} content, which may be attributed to the larger ionic radii of Ni^{2+} (0.69 Å) than Mg^{2+} (0.65 Å). However, the crystallite size seems to be independent of Ni content, and averaged to

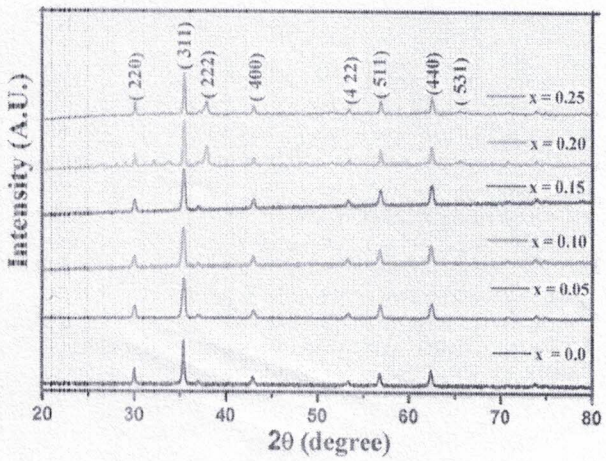

Fig. 1. X-ray diffraction patterns of the sintered $Mg_{0.25-x}Ni_xCu_{0.25}Zn_{0.5}Fe_2O_4$ ferrites.

Table 1
Lattice parameter (a), crystallite size (t), bulk density (ρ_m), X-ray density (ρ_x) and relative density (ρ_R) of sintered $Mg_{0.25-x}Ni_xCu_{0.25}Zn_{0.5}Fe_2O_4$ ferrites.

X	a (Å)	t (nm)	ρ_m (gm/cm^3)	ρ_x (gm/cm^3)	ρ_R (%)
0	8.381 ± 0.002	45 ± 0.2	4.56 ± 0.2	5.19 ± 0.08	88 ± 1
0.05	8.389 ± 0.001	48 ± 0.2	5.01 ± 0.1	5.22 ± 0.06	96 ± 1
0.10	8.394 ± 0.002	46 ± 0.1	4.97 ± 0.2	5.24 ± 0.06	95 ± 0.5
0.15	8.396 ± 0.002	49 ± 0.2	4.96 ± 0.2	5.28 ± 0.04	94 ± 0.5
0.20	8.409 ± 0.003	46 ± 0.1	4.76 ± 0.1	5.29 ± 0.07	90 ± 0.8
0.25	8.411 ± 0.003	47 ± 0.3	4.74 ± 0.1	5.33 ± 0.05	89 ± 0.4

45–49 nm. The synthesized materials possesses the relative density of > 88%, due to Cu (by promoting the lattice diffusion of cations) [18–20]. In addition, X-ray density of each sintered sample was observed to be higher than the corresponding bulk density due to the existence of pores and lower sintering temperature [21]. Fig. 2 illustrates the typical porous morphology of ferrites with some voids and empty spaces. The average grain size (line intercept method, Table 2) revalidated the XRD results. The presence of Cu affects the microstructure due to liquid phase sintering, which facilitates the grain growth [22]. The nonhomogeneous driving force on the grains resulted into nonuniform grain size distribution (TEM, Fig. 3) [23–25]. Further, the SAED patterns (insets Fig. 3) reflected polycrystalline nature of the ferrites, revalidating XRD results. Elemental analysis (EDS) of shows the presence all desired constituent elements (Table S1, Fig. 4). The elemental composition was found to be in good agreement with the initial concentration.

In the following, electrical properties of developed ferrites are represented (Fig. 5). The room temperature DC resistivity of ferrites was found above 10^6 Ω-cm. With increasing temperature up to 350 °C, the resistivity of the material got decreased (Fig. 5.a). The resistivity was found to increase with Ni content up to x = 0.15, and then decreased with further increase in Ni. The activation energies for different regions i.e. ferro and para and Curie temperature (Tc) are tabulated in Table 2. Fig. 5.b–e shows the dielectric properties, the dielectric constants (ε′ and ε″) were found to decrease rapidly with an increase in initial frequency, and remained constant at higher frequencies (Fig. 5.b,c). Due to electronic exchange of $Fe^{2+} \leftrightarrow Fe^{3+}$, the local displacement of electrons in the direction of applied electric field, induced the polarization in ferrites [26]. Beyond a fixed frequency of electric field, the electron exchange does not follow the fast alternating field, and thereby remained constant at higher frequency. The dielectric losses in ferrites are generally gets reflected in the resistivity i.e. materials with low resistivity exhibit high dielectric loss and vice versa, which has been observed in the present case (Fig. 5.d) [27]. The ac resistivity of developed ferrites is depicted in Fig. 5.e. The room temperature ac resistivity was found to be influenced by addition of Ni. The sample with x = 0.05 exhibited highest ac resistivity.

Fig. 6 illustrates the magnetic properties of the developed ferrites. The normalized AC susceptibility of ferrites remained invariant, and displayed sudden drop near the Curie-temperature (Fig. 6.a). The decreasing trend in susceptibility with temperature confirmed the ferrimagnetic nature of the material. Up to Curie-temperature the available thermal energy was not quite sufficient to disturb the aligned moments of the spins. However, near the transition-temperature, the thermal energy is high enough to disturb all the aligned spins, where the susceptibility decreased drastically, and transforms into the paramagnetic region. The Curie-temperature was found to increase with increasing Ni content (Table 2), due to enhancement in ferrimagnetic region (ordered state) at the expense of the paramagnetic region. Further, the room temperature susceptibility was found to increase with Ni addition, due to higher magnetic moment of Ni^{2+}. The material exhibited a typical magnetic hysteresis loop (Fig. 6.b), indicating ordered soft ferromagnetic nature. The saturation magnetization and coercivity were found to increase with Ni content (Table 3), due to replacement of nonmagnetic

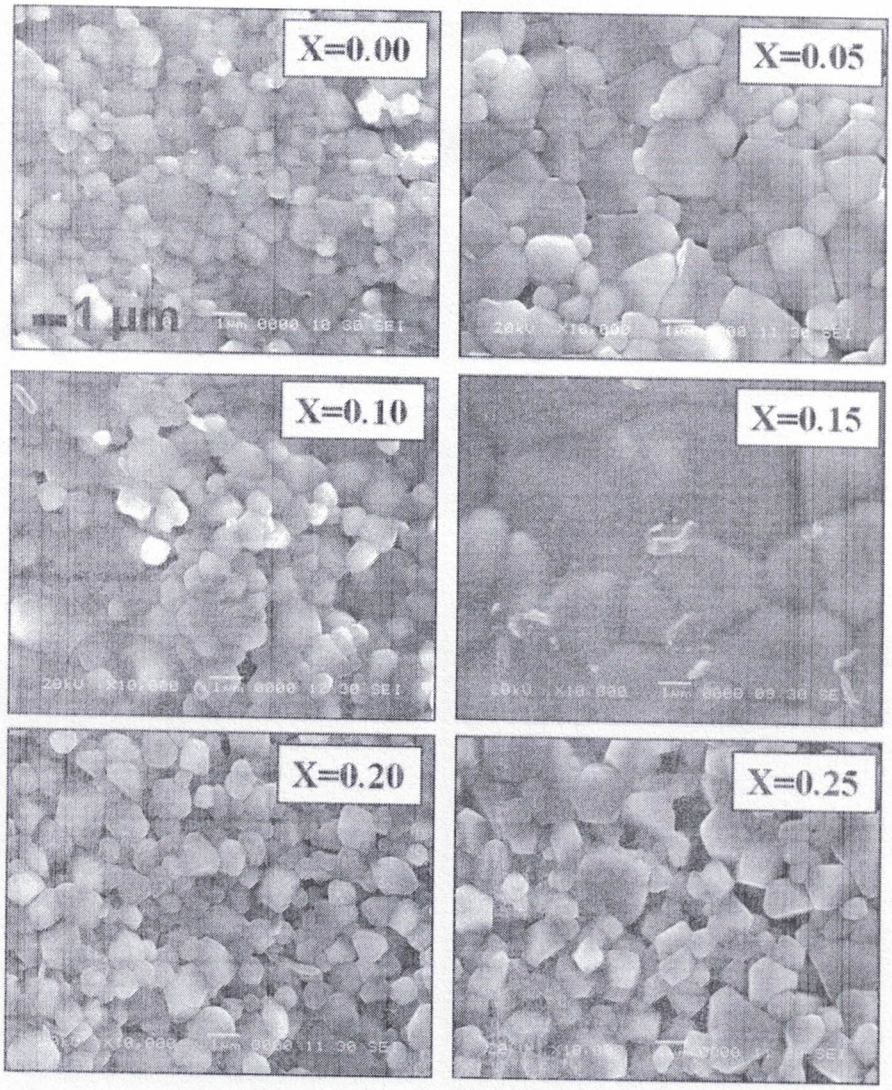

Fig. 2. SEM images of sintered $Mg_{0.25-x}Ni_xCu_{0.25}Zn_{0.5}Fe_2O_4$ ferrites.

Table 2
Grain size, particle size from TEM, activation energy, Curie temperature (T_C) of sintered $Mg_{0.25-x}Ni_xCu_{0.25}Zn_{0.5}Fe_2O_4$ ferrites.

X	Grain size (μm)	Particle size (nm)	Activation energy (eV)		T_C (°C)
			Ferro	Para	
0	0.91 ± 0.1	314 ± 3	0.28 ± 0.03	0.58 ± 0.03	143 ± 1
0.05	1.48 ± 0.1	129 ± 2	0.35 ± 0.03	0.57 ± 0.03	151 ± 2
0.10	0.98 ± 0.2	203 ± 2	0.40 ± 0.02	0.66 ± 0.02	185 ± 4
0.15	2.68 ± 0.2	205 ± 1	0.46 ± 0.02	0.65 ± 0.02	205 ± 3
0.20	1.11 ± 0.1	123 ± 3	0.49 ± 0.03	0.70 ± 0.03	222 ± 2
0.25	1.03 ± 0.2	90 ± 2	0.61 ± 0.04	0.89 ± 0.04	232 ± 1

Mg^{2+} ions with magnetic Ni^{2+} ions. Also, Mg preferably occupies B-site, and due to Ni substitution in place of Mg, an increase in the magnetization on octahedral sublattice takes place, leading to increase in saturation magnetization of the ferrite [28]. The probable cation distribution and experimental magnetic moments are given in Table S2. Initial permeability is known to be one of the most sensitive magnetic properties of ferrites. In the present investigations, initial permeability (μ_i) value remained almost constant up to a particular frequency, beyond which it started to increase (Fig. 6.c). The room temperature values of μ_i at 1 KHz are given Table S3. The samples with Ni content > 0.05, μ_i got decreased due to an increase in the magnetostriction constant by substitution of Mg by Ni [29]. Further, Ni is a traditional magnetostrictive material with high magnetostrictive coefficient at low magnetic bias. Due to soft magnetic nature, it enhances the magnetostrictive properties of Mg, Cu, and Zn. Fig. 6.d shows the temperature dependence of initial permeability of developed ferrites. Unlike frequency dependency, μ_i value remained almost constant up to a particular temperature, beyond which it started to decrease. The temperature at which this abrupt fall tool place is the magnetic Curie transition temperature (T_c). It is usually ascribed as the magnetic transition (ferromagnetic-to-paramagnetic). The magnitude of T_c increased with increase in Ni content and is attributed to the replacement of non-magnetic Mg^{2+} ion by Ni^{2+} ions [30]. The values of rotational permeability (Table S4) and wall permeability have been calculated using formula:

$$\mu_{rk} = 1 + 2\pi M^2 s/k_1 \quad (1)$$

$$\mu_w = \mu_i - (\mu_{rk} - 1) \quad (2)$$

where, Ms: saturation magnetization, K_1: anisotropy constant, μ_{rk}: rotational permeability, and μ_w: wall permeability. Fig. 6.e shows variation of loss factor as function of temperature. The loss factor got increased at higher temperature range. It is well known that higher the μ_i

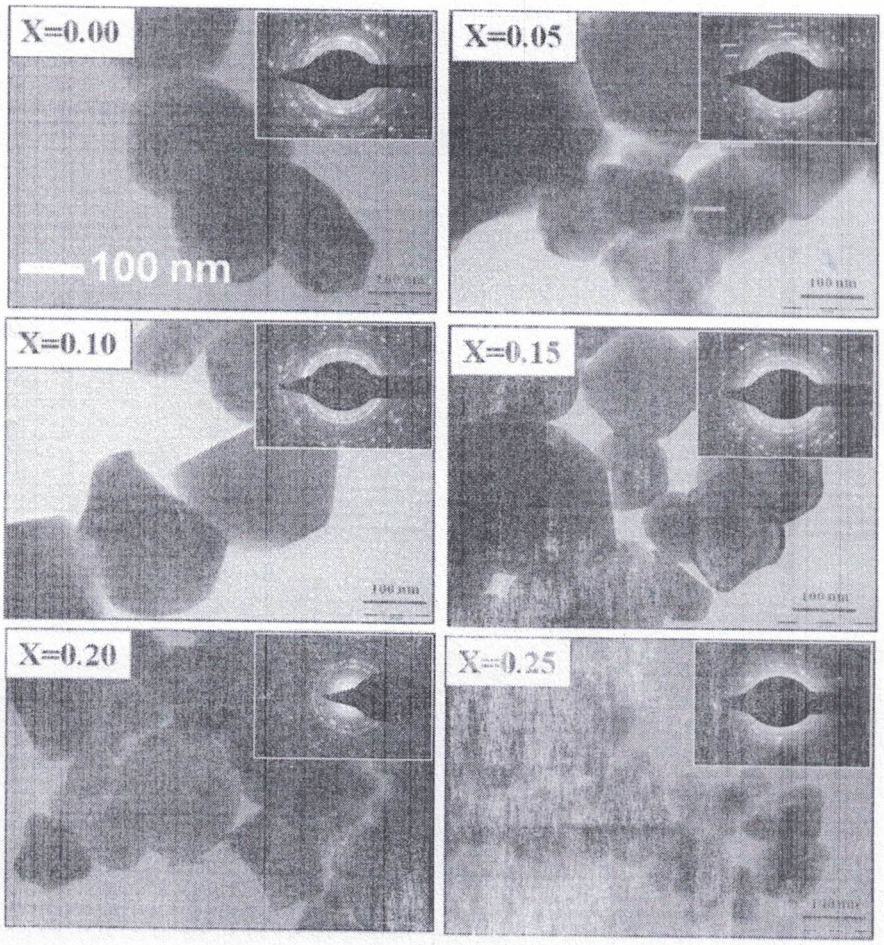

Fig. 3. TEM and SAED patterns (inset) of sintered $Mg_{0.25-x}Ni_xCu_{0.25}Zn_{0.5}Fe_2O_4$ ferrites.

value, lower is the loss factor, which is in the fitness of obtained results.

As there are no direct reports available on Ni^{2+} substituted Mg-Cu-Zn ferrite for comparing the obtained results, it is rather cumbersome to make the spreadsheet of all the investigated properties. Therefore, authors are restricted themselves to compare the results on magnetic properties, which is the core of the present investigation (Table 4).

4. Conclusions

We have developed a simple route for the synthesis of Ni substituted Mg-Cu-Zn ferrite. The doping level of Ni is varied in the range of $0 \le x \le 0.25$ in step 0.05, where the system is $Mg_{0.25-x}Ni_xCu_{0.25}Zn_{0.5}Fe_2O_4$. MSS method yielded into a cubic spinel structure

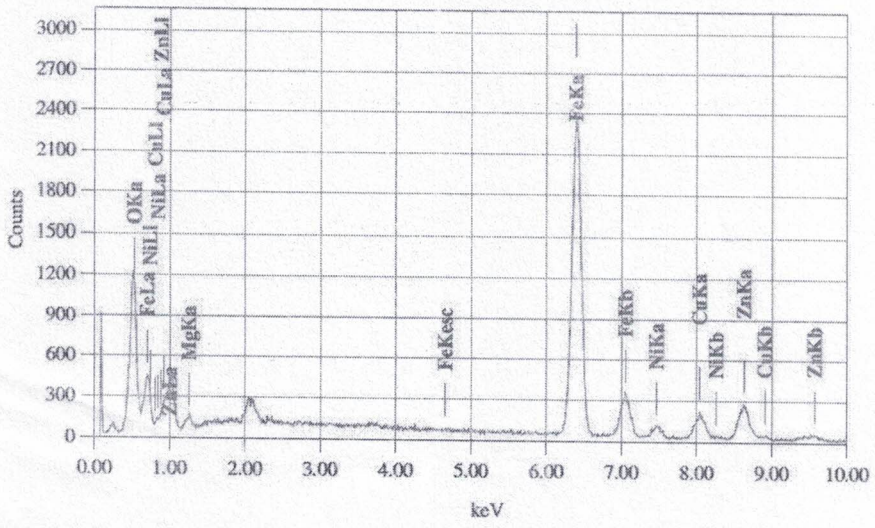

Fig. 4. EDS spectrum of sintered $Mg_{0.25-x}Ni_xCu_{0.25}Zn_{0.5}Fe_2O_4$ ferrites.

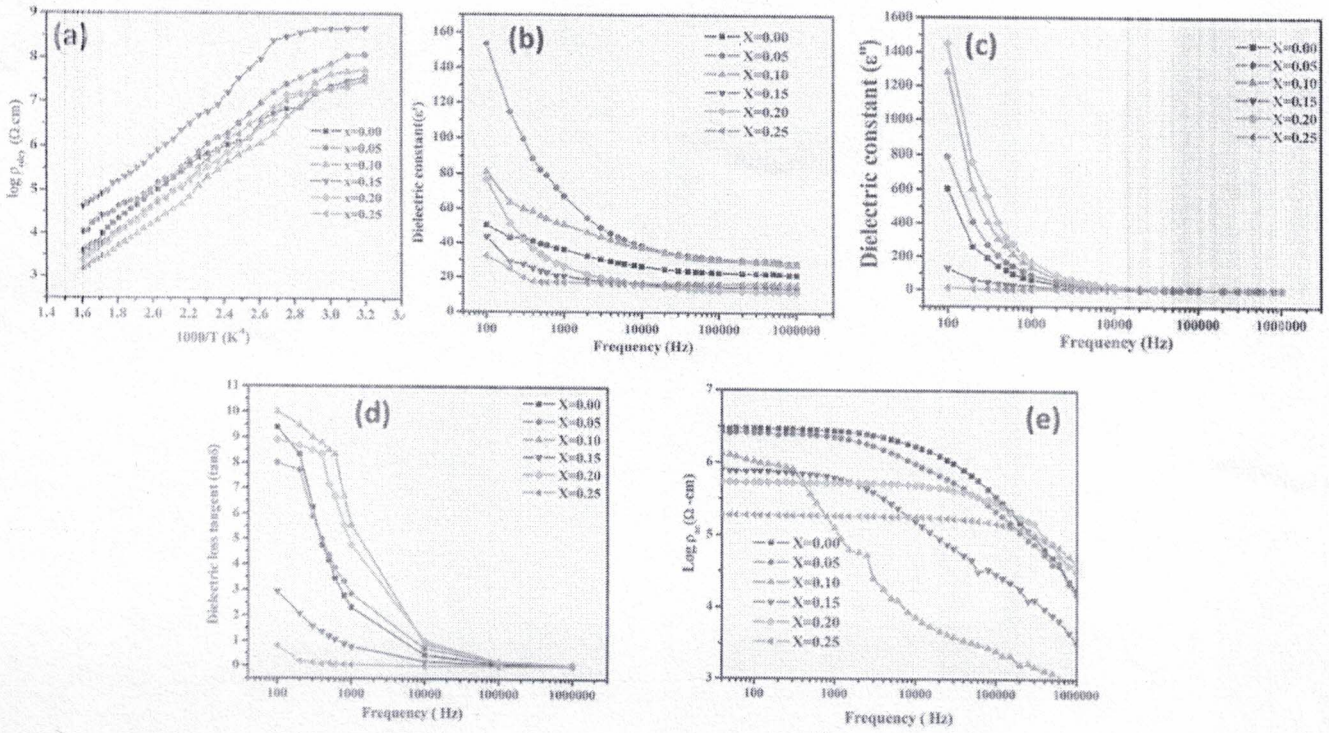

Fig. 5. Electrical properties of the developed ferrites. a) DC resistivity, b,c) dielectric constants (ε′ and ε″), d) dielectric loss tangent, and e) ac resistivity.

along with expansion of the unit cell of Mg-Cu-Zn ferries due to Ni^{2+} addition. Microstructure revealed the formation of dense microstructures with vivid grains. The electric transport, dielectric and magnetic properties were strongly found to be dependent on Ni content. The investigated dielectric and magnetic properties showed that the $Mg_{0.25-x}Ni_xCu_{0.25}Zn_{0.5}Fe_2O_4$ ferrite with X = 0.05 can be the potential candidate for MLCI application with low sintering temperature in view of high density, high initial permeability and saturation magnetization possessed by that composition.

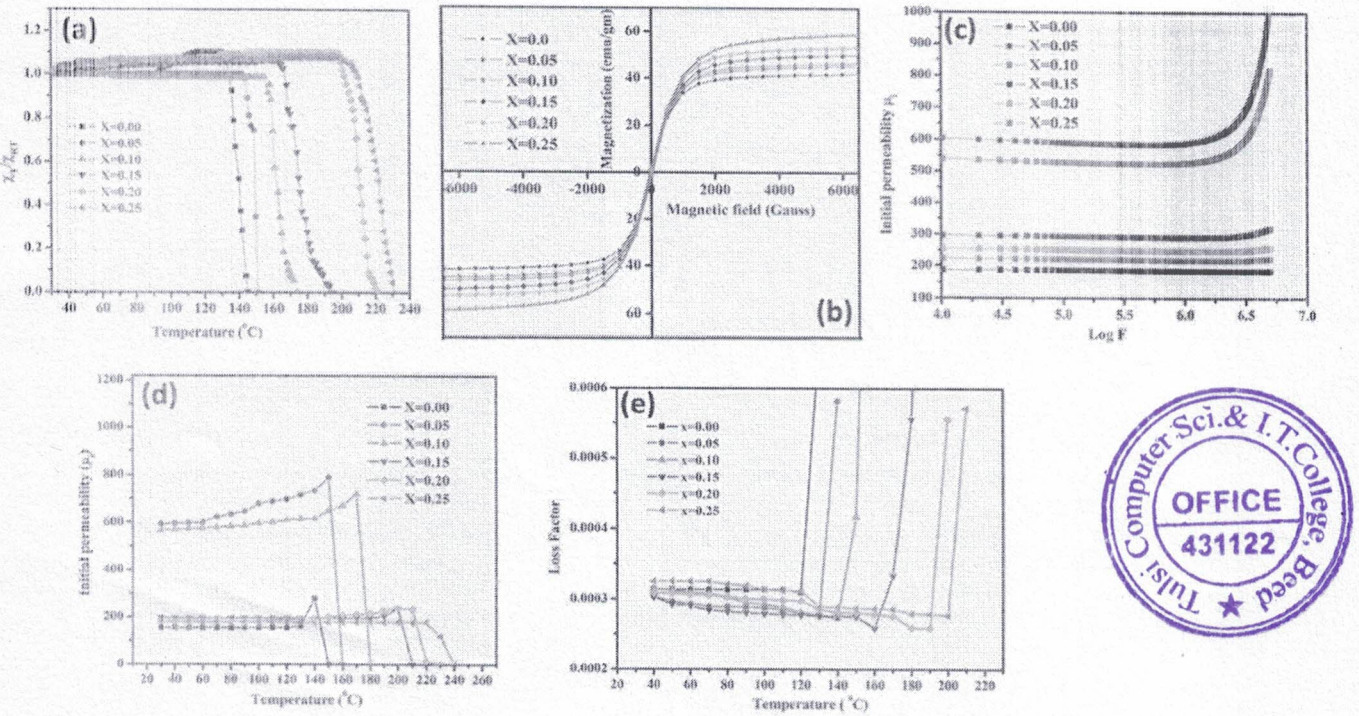

Fig. 6. Magnetic properties of ferrites. a) A.C. susceptibility, b) magnetization-(VSM), c,d) initial permeability (frequency and temperature dependency), and e) loss factor.

Table 3
Data on magnetic parameters like M_s, Mr/Ms, n_B, Hc and relative density (ρ_R) and Curie temperature (T_C) for different compositions of sintered $Mg_{0.25-x}Ni_xCu_{0.25}Zn_{0.5}Fe_2O_4$ ferrites.

X	M_s (emu)	M_r/M_s	n_B Expt.	ρ_R (%)	H_c G	T_C (°C) $\chi_{a.c.}$
0.00	220 ± 2	0.0076	1.76 ± 0.05	88 ± 1	6.97 ± 1	145 ± 2
0.05	240 ± 1.5	0.0090	1.91 ± 0.02	96 ± 2	8.92 ± 1.5	151 ± 2
0.10	248 ± 2	0.0100	1.97 ± 0.02	95 ± 0.5	10.37 ± 1.3	174 ± 3
0.15	270 ± 3	0.0170	2.15 ± 0.03	94 ± 1	17.13 ± 1	194 ± 4
0.20	288 ± 7	0.0180	2.28 ± 0.05	90 ± 1.4	18.89 ± 0.5	220 ± 2
0.25	325 ± 5	0.0330	2.58 ± 0.04	89 ± 2	36.86 ± 5	231 ± 6

Table 4
Comparative data on magnetic properties of Ni^{2+} substituted Mg-Cu-Zn ferrite synthesized using molten salt and citrate-gel combustion routes.

#	Adopted synthesis method	Magnetic properties		
		M_s (emu)	H_c G	$K_1 \times 10^4$ (erg/cc)
1	Molten salt	220	6.97	−2.50
2	Citrate gel combustion	239	3.41	−2.50

Conflict of interest

The authors declare that they have no conflict of interest.

Appendix A. Supplementary material

Supplementary data to this article can be found online at https://doi.org/10.1016/j.inoche.2018.11.003.

References

[1] L. Leontie, C. Doroftei, Nanostructured spinel ferrites for catalytic combustion of gasoline vapors, Catal. Lett. 147 (10) (2017) 2542.
[2] M. Ansari, A. Baykal, S. Asiri, S. Rehman, Synthesis and characterization of antibacterial activity of spinel chromium-substituted copper ferrite nanoparticles for biomedical application, J. Inorg. Organomet. Polym. (2018), https://doi.org/10.1007/s10904-018-0889-5.
[3] R. Sharma, P. Thakur, P. Sharma, V. Sharma, Ferrimagnetic Ni^{2+} doped Mg-Zn spinel ferrite nanoparticles for high density information storage, J. Alloys Compd. 704 (7) (2017).
[4] M. Amiri, A. Pardakhti, M. Ahmadi-Zeidabadi, A. Akbari, M. Salavati-Niasari, Magnetic nickel ferrite nanoparticles: green synthesis by *Urtica* and therapeutic effect of frequency magnetic field on creating cytotoxic response in neural cell lines, Colloids Surf. B 172 (2018) 244.
[5] M. Amiri, M. Ahmadi, A. Pardakhti, M. Salavati-Niasari, Synthesis and in vitro evaluation of a novel magnetic drug delivery system: proecological method for the preparation of $CoFe_2O_4$ nanostructures, J. Mol. Liq. 249 (2018) 1151.
[6] M. Amiri, M. Salavati-Niasari, A. Pardakhty, M. Ahmadi, A. Akbari, Caffeine: a novel green precursor for synthesis of magnetic $CoFe_2O_4$ nanoparticles and pH-sensitive magnetic alginate beads for drug delivery, Mater. Sci. Eng. C 76 (2017) 1085.
[7] M. Amiri, M. Salavati-Niasari, A. Akbari, T. Gholami, Removal of malachite green (a toxic dye) from water by cobalt ferrite silica magnetic nanocomposite: herbal and green sol-gel autocombustion synthesis, Int. J. Hydrog. Energy 42 (2017) 24846.
[8] A. Shan, X. Wu, J. Lu, Phase formations and magnetic properties of single crystal nickel ferrite ($NiFe_2O_4$) with different morphologies, CrystEngComm 17 (2015) 1603.
[9] X. Lasheras, M. Insausti, I. Muro, E. Garaio, F. Plazaola, M. Moros, J. Martinez de la Fuente, L. Lezama, Chemical synthesis and magnetic properties of monodisperse nickel ferrite nanoparticles for biomedical applications, J. Phys. Chem. C 120 (6) (2016) 3492.
[10] Y. Xu, D. Sun, H. Hao, D. Gao, Y. Sun, Non-stoichiometric Co(II), Ni(II), Zn(II)-ferrite nanospheres: size controllable synthesis, excellent gas-sensing and magnetic properties, RSC Adv. 6 (2016) 98994.
[11] J. Patil, D. Nadargi, I. Mulla, S. Suryavanshi, Spinel $MgFe_2O_4$ thick films: a colloidal approach for developing gas sensors, Mater. Lett. 213 (2018) 27.
[12] M. Amiri, M. Salavati-Niasari, A. Akbari, A magnetic $CoFe_2O_4/SiO_2$ nanocomposite fabricated by the sol-gel method for electrocatalytic oxidation and determination of L-cysteine, Microchim. Acta 184 (2017) 825.
[13] M. Amiri, M. Salavati-Niasari, A. Akbari, R. Razavi, Sol–gel auto-combustion synthesize and characterization of a novel anticorrosive cobalt ferrite nanoparticles dispersed in silica matrix, J. Mater. Sci. Mater. Electron. 28 (2017) 10495.
[14] M. Salavati-Niasari, M. Shaterian, M.R. Ganjali, P. Norouzi, Oxidation of cyclohexene with tert-butylhydroperoxide catalysted by host (nanocavity of zeolite-Y)/guest (Mn(II), Co(II), Ni(II) and Cu(II) complexes of N,N′-bis(salicylidene)phenylene-1,3-diamine) nanocomposite materials (HGNM), J. Mol. Catal. A Chem. 261 (2007) 147.
[15] M. Salavati-Niasari, F. Farzaneh, M. Ghandi, Oxidation of cyclohexene with tert-butylhydroperoxide and hydrogen peroxide catalyzed by alumina-supported manganese (II) complexes, J. Mol. Catal. A Chem. 186 (2002) 101.
[16] S.M. Hosseinpour-Mashkani, F. Mohandes, M. Salavati-Niasari, K. Venkateswara-Rao, Microwave-assisted synthesis and photovoltaic measurements of $CuInS_2$ nanoparticles prepared by using metal-organic precursors, Mater. Res. Bull. 47 (2012) 3148.
[17] M. Khandekar, N. Tarwal, I. Mulla, S. Suryavanshi, Nanocrystalline Ce doped $CoFe_2O_4$ as an acetone gas sensor, Ceram. Int. 40 ((1) (2014) 447.
[18] M. Salavati-Niasari, Synthesis and characterization of host (nanodimensional pores of zeolite-Y)-guest [unsaturated 16-membered octaaza-macrocycle manganese(II), cobalt(II), nickel(II), copper(II), and zinc(II) complexes] nanocomposite materials, Chem. Lett. 34 (2005) 1444.
[19] M. Penchal Reddy, I. Kim, Effect of La substitution on structural and magnetic properties of microwave treated $Mg_{0.35}Cu_{0.05}Zn_{0.60}La_xFe_{2-x}O_4$ ceramics, Superlattice. Microst. 56 (2013) 99.
[20] G. Kianpour, M. Salavati-Niasari, H. Emadi, Sonochemical synthesis and characterization of $NiMoO_4$ nanorods, Ultrason. Sonochem. 20 (2013) 418.
[21] R. Coble, T. Gupta, G. Kuczynski, N. Hroton, C. Gibbon (Eds.), Sintering and Related Phenomena, Gordon and Breach, New York, 1967, p. 423.
[22] K. Low, F. Sale, Electromagnetic properties of gel-derived NiCuZn ferrites, J. Magn. Magn. Mater. 246 (2002) 30.
[23] S. Zinatloo-Ajabshir, M. Salavati-Niasari, M. Hamadanian, Praseodymium oxide nanostructures: novel solvent-less preparation, characterization and investigation of their optical and photocatalytic properties, RSC Adv. 5 (2015) 33792.
[24] E. Esmaeili, M. Salavati-Niasari, F. Mohandes, F. Davar, H. Seyghalkar, Modified single-phase hematite nanoparticles via a facile approach for large-scale synthesis, Chem. Eng. J. 170 (2011) 278.
[25] Y. Hayashi, T. Kimura, T. Yamaguchi, Preparation of rod-shaped $BaTiO_3$ powder, J. Mater. Sci. 21 (1986) 757.
[26] C. Kolekar, P. Kamble, S. Kulkurni, A. Vaingamkar, Effect of Gd^{3+} substitution on dielectric behaviour of copper-cadmium ferrites, J. Mater. Sci. 30 (1995) 5784.
[27] A.S. Hudson, Substitution of gadolinium, aluminium, and indium in yttrium calcium vanadium garnets, IEEE Trans. Magn. 5 (3) (1969) 610.
[28] J. Smit, H.P.J. Wijn, Ferrites, Philips Technical library, Eindhoven, Holland, 1959.
[29] J. Nam, W. Han, J. Oh, The effect of Mn substitution on the properties of NiCuZn ferrites, J. Appl. Phys. 81 (8) (1997) 4794.
[30] M. Naeem, N. Shah, I. Gul, A. Maqsood, Structural, electrical and magnetic characterization of Ni–Mg spinel ferrites, J. Alloys Compd. 487 (2009) 739.